Nuclear structure effects in the sub-barrier fusion of $^{16}O + {}^{70,72,73,74,76}Ge$

E. F. Aguilera
Departamento de Aceleradores, Instituto Nacional de Investigaciones Nucleares, A. P. 18-1027, C.P. 11801, Mexico, D. F., Mexico

J. J. Kolata and R. J. Tighe*
Physics Department, University of Notre Dame, Notre Dame, Indiana 46556
(Received 24 February 1995)

Fusion excitation functions were obtained for $^{16}O + {}^{70,72,73,74,76}Ge$ at energies from about 4 MeV below to 15 MeV or more above the Coulomb barrier. The barrier parameters extracted from the data agree within 2% with those obtained from the systematics for fusion above the barrier. Low-energy enhancements are observed whose behavior is explained within the context of simple model calculations by assigning appropriate degrees of freedom to the respective reaction partners. These degrees of freedom are consistent with those used in similar analysis of different data sets where either the same projectile or the same targets were used. An analysis of the barrier distributions is made which supports the previous conclusions.

PACS number(s): 25.70.Jj

I. INTRODUCTION

The idea that nuclear structure might play an important role in the process of sub-barrier fusion of heavy ions has been well accepted for some time [1]. It has been shown that the internal degrees of freedom of the reactant nuclei can provide favored channels to fusion and that this can explain the enhanced cross sections observed for many systems with respect to the predictions of the one-dimensional barrier penetration models (BPM's).

Some of the most common degrees of freedom that have been considered in this context are surface vibrations [2], particle transfer [3], static deformation [4], neck formation [5], and quasimolecular excitations [6]. Coupling to any of these kinds of channels will in general produce an enhancement of the sub-barrier fusion cross sections over the BPM predictions. However, the relevant degrees of freedom are still not known for a large number of systems.

In a previous work [7], we reported our observations that the sub-barrier fusion excitation functions for $^{27}Al + {}^{70,72,73,74,76}Ge$ show some quite interesting effects. The data clearly suggested a structural change between $^{70,72}Ge$ and $^{73,74,76}Ge$. The larger enhancement for $^{27}Al + {}^{73}Ge$ with respect to $^{27}Al + {}^{70,72}Ge$ was explained by assuming that all three Ge isotopes are spherical vibrators and noticing that the ^{73}Ge nucleus has more low-lying collective inelastic channels that can be coupled to the ground state with appreciable strength because of its odd-A nature. For the case of $^{27}Al + {}^{74,76}Ge$, on the other hand, the larger enhancement could be explained as the consequence of a transition from spherical (or possibly oblate) shapes for $^{70,72}Ge$ to prolate deformed shapes for $^{74,76}Ge$. For the ^{27}Al projectile, a statically deformed oblate shape was used in the model calculations. Only one free parameter, the depth of the nuclear ion-ion potential, was used in the calculations and the scheme arrived at in that work was consistent with previous spectroscopic information about the targets and the projectile.

The method of analysis, which produced excellent quantitative agreement with the data, was in later works [8,9] successfully used to describe the reported fusion data [10,11] for the independent systems $^{16}O + {}^{147-150,152,154}Sm$. It is well known that these Sm isotopes are characterized by an increasing static deformation with mass number. The introduction of the corresponding prolate deformation, as it turned out, was not enough to account for the large enhancements observed for these systems. The contribution of the surface vibrational degrees of freedom for ^{16}O turned out to be essential in order to properly describe the data. Essentially the same conclusion was reached by Gomes *et al.* [12] in a recent analysis concerning the $^{16}O + {}^{154}Sm$ system which included, in addition to the data of Ref. [10], some newer measurements by Wei *et al.* [13]. Some later analysis [14,15] resolved the discrepancy between the quadrupole deformation parameter β_2 extracted from the fusion data in Ref. [13] and that from Coulomb excitation by including in the calculation, in addition to β_2, a hexadecapole deformation β_4. Although no internal degree of freedom of ^{16}O was invoked in the analysis in order to describe the data, there still exists the possibility that equally good fits might be achieved by incorporating them. As pointed out by Morton *et al.* [16], in the presence of strong coupling effects (such as the large static deformation of ^{154}Sm), the small perturbations caused by relatively weaker couplings (such as the ^{16}O excitations) are difficult to identify unambiguously. It is worthwhile to mention at this point that a coupled-channels treatment (which properly simulates the fusion process) of the elastic and inelastic scattering of ^{16}O on $^{40,48}Ca$, ^{58}Ni, and ^{88}Sr has shown [17] that the 2^+ and 3^- states in ^{16}O have a significant influence on the calculated cross sections.

The results mentioned in the two previous paragraphs motivated us to measure the combined $^{16}O + {}^{70,72,73,74,76}Ge$ systems. The main purpose was to investigate whether the same degrees of freedom, determined independently for O and Ge in the previous works, were suitable to properly describe the combined O+Ge systems. Some preliminary results [9,18] seemed to confirm this hypothesis for the case of

*Present address: Bldg. 88, Lawrence Berkeley Lab., Berkeley, CA 94720.

TABLE I. Characteristics of the targets used in this work. The ^{72}Ge target was self-supporting.

	Carbon			
Target	Thickness (μg/cm^2)	Backing (μg/cm^2)	Isotopic composition (percent of ^{70,72,73,74,76}Ge)	Notes
^{70}Ge	250 (8)	20	96.75, 1.12, 0.29, 1.36, 0.48	a, d
^{72}Ge	565 (15)	- - -	1.04, 96.23, 0.77, 1.63, 0.33	b
^{73}Ge	115 (12)	40	0.86, 2.09, 94.50, 2.24, 0.31	c, d
^{74}Ge	110 (9)	20	1.71, 2.21, 0.90, 94.48, 0.70	c, d
^{76}Ge	143 (10)	20	7.69, 6.65, 1.69, 10.08, 73.89	a, d

[a]Target thickness determined by energy-loss measurements of α particles from a ^{228}Th source.
[b]Target thickness determined by energy-loss measurements of 57.5 MeV ^{16}O ions.
[c]Target thickness determined by energy-loss measurements of α particles from a ^{241}Am source.
[d]GeO_2.

^{16}O + ^{72,73}Ge but not for ^{16}O + ^{74}Ge. In this work, this last system has been remeasured and the analysis of all five systems has been completed.

II. EXPERIMENTAL PROCEDURE AND RESULTS

Beams of ^{16}O from the tandem FN Van de Graaff accelerator at the University of Notre Dame were used to bombard targets of ^{70,72,73,74,76}Ge at laboratory energies in the region from 38 to 66 MeV, in steps of 1 MeV. The characteristics of the targets are listed in Table I.

The evaporation residues (ER's) were detected in a recoil velocity spectrometer (see Fig. 1) whose main components are an electrostatic deflector, to separate the residues from the transmitted beam, and a time-of-flight–energy telescope which allows us to identify their mass. Further details of the spectrometer can be found in Refs. [7] and [19]. The transmission efficiency of the ER's through the recoil velocity spectrometer was determined empirically by elastic scattering of ions of similar atomic and mass numbers. To accomplish this, we measured the Rutherford scattering of ^{81}Br ions on ^{70}Ge at a laboratory angle of 10.4° and at bombarding energies of 8, 10, and 12 MeV, chosen to cover the experimental energy range of the ER's. The results indicated that the transmission probability for these slow ions is energy dependent, ranging from about 49% at the lowest energies to 56% at the highest energies. In order to account for this energy dependence, a straight line was fit to the empirical transmission points as a function of the output energy when the ion exits the target. The linear correlation coefficient for this fit was 0.98. An estimation for this energy was then made for each measured point in the O+Ge systems, by assuming a ^{81}Br residue and using appropriate energy-loss corrections for both the projectile and the residue. A Monte Carlo model which simulated the performance of the spectrometer was used to check that the transmission is not a sensitive function of the mass of the ER's. For example, using residues of either ^{90}Zr or ^{81}Br for the case of the ^{16}O+^{76}Ge system gave consistent results for the transmission. Our choice of the ^{81}Br residue for all systems in the above-mentioned estimation is thus expected to give accurate results.

The simultaneous measurement of Rutherford scattering of the beam with a four-monitor system allowed us to obtain absolute normalization factors for the differential cross sections with high precision ($\sim$ 1%). We have shown [20] that, in contrast to the usual method where only one monitor is used (or the less usual one with two monitors), this method gives results which are stable against variations in the alignment of the detector system or beam-focusing conditions. Even for the case of a reasonably good alignment, the precision obtained with our system is typically about 20 (4) times better than that of the one- (two-) monitor method.

Since particle evaporation is the dominant decay mode for

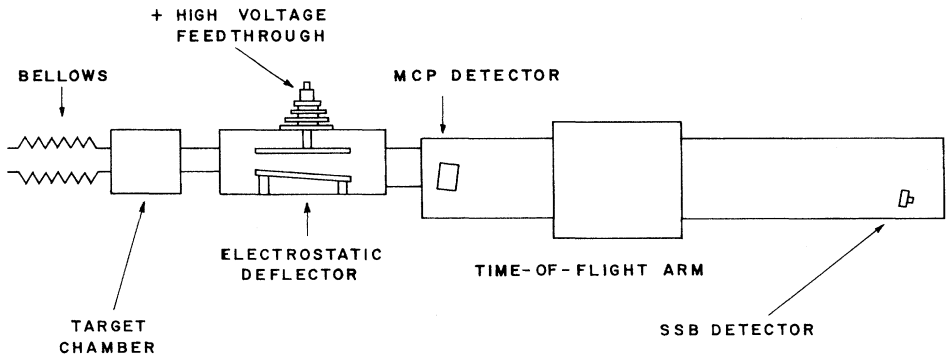

FIG. 1. Schematic side view of the recoil velocity spectrometer.

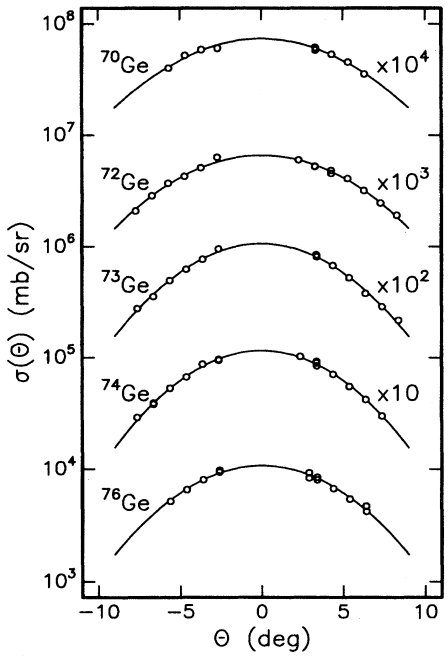

FIG. 2. Angular distributions obtained for ^{16}O + ^{70,72,73,74,76}Ge at $E_{\text{c.m.}}$ = 40.3, 40.1, 40.8, 40.9, and 41.1 MeV, respectively. The error bars are smaller than the points in all cases. The widths (standard deviations) of the fitted Gaussians (solid lines) are 5.3° , 5.2°, 4.6°, 4.5°, and 4.7°, respectively.

compound nuclei in the present mass and energy range, the complete fusion cross sections were simply taken as the ER cross sections. We measured single-angle excitation functions, at an angle of 3° , which were then normalized to integrated angular distributions obtained at selected energies. As the shape of these angular distributions does not change appreciably within the energy range covered by our experiments, this procedure is well justified. A set of angular distributions typical of each system is presented in Fig. 2. Since these distributions are symmetric around $\theta=0°$, the measurement of positive and negative angles allows for interpolation to the important region of small angles, while determining at the same time the zero-degree position of the time-of-flight arm with high precision. The results of Gaussian fits to the data are shown as solid curves in Fig. 2, with the corresponding widths indicated in the caption. It might seem surprising at first sight to find no substantial effect of the target thickness on these widths since, for example, the ^{72}Ge target has a thickness which is about a factor of 5 larger than that of ^{74}Ge and a factor of 2 larger than that of ^{70}Ge. We made some rough estimations of multiple scattering effects by using the widths reported in Ref. [21]. An effective target thickness for fusion residues was calculated by evaluating the mean depth at which fusion occurs, obtaining 129, 297, 58, 56, and 73 μg/cm^2 for ^{70,72,73,74,76}Ge, respectively. Representative Br residues were assumed for all cases, with respective energies determined from momentum conservation. Assuming that the contributions of different elements in the target add quadratically, the angular straggling semi-widths (standard deviations of equivalent Gaussians) estimated for the ^{70,72,73,74,76}Ge targets were 1.4°, 3.1°, 0.9°, 0.8°, and 1.0°, respectively. If we assume in addition that the kinematic spread of the residues adds quadratically with the angular straggling to produce the experimental widths, the previous values are consistent with a kinematic spread of about 4.6° for all targets, with a maximum fluctuation of $\pm 0.5°$, a quite reasonable result if we consider that different evaporation residues with different energies might be expected for each target. We conclude, therefore, that multiple scattering in the target is not a big effect even for the thickest target. Integration of the Gaussian distributions over the whole solid angle gave total fusion cross sections for the selected energies, which were then used to scale the single-angle excitation functions.

Impurities in the isotopic composition of the targets, and the energy loss in them, were accounted for as described in Ref. [7]. The resulting fusion cross sections are listed in Tables II and III. The reported errors include the 2% uncertainty in the absolute normalization factors as well as the statistical errors. In addition, a maximum systematic error of about 7% is estimated for our data coming mainly from the transmission efficiency determination (~5%), the scaling of single-angle excitation functions (~2%), and the observation-angle error of the spectrometer (~5%). Since the corrections for isotopic impurities were very small for most data points, we neglected the corresponding contribution to the systematic error. The data are displayed in Fig. 3 for all systems, together with model calculations which will be discussed in the next sections.

III. METHODOLOGY

In order to investigate the effects of surface vibrations and/or static deformations, a modified version of the simplified coupled-channels code CCDEF was used. In CCDEF [22] the vibrational states are coupled to the ground state by using the constant coupling approximation, in which the resulting fusion cross sections can be written as a weighted sum of Wong-type cross sections [23] calculated for different barrier heights. Static deformation effects, on the other hand, are treated in the code through the equivalent-spheres method. In brief, the nuclear radii of deformed nuclei depend on the deformation parameters and on the orientation angles with respect to the collision axis, and through them the nuclear and Coulomb potentials depend also on these variables. The cross section is calculated for each pair of relative angles, and the final result is obtained by averaging over all possible orientations.

A Woods-Saxon well with one free parameter (the well depth) is used for the nuclear ion-ion potential. The corresponding radius and diffuseness were fixed at $R=R_p+R_t+0.29$ fm and $a=0.63$ fm, where the projectile and target radii are calculated according to

$$R_{p,t}=1.233A_{p,t}^{1/3}-0.978A_{p,t}^{-1/3}\ \text{fm}\,. \tag{1}$$

In the present version of CCDEF a fitting procedure was introduced so that the free parameter is allowed to vary until the best fit to an experimental excitation function is achieved. Unlike previous works [7,9,18], where one-dimensional BPM calculations were fit only to experimental points with cross section values between 100 and 500 mb, all

TABLE II. Total fusion cross sections for $^{16}O+^{70,72,73}Ge$.

System	$E_{c.m.}$ (MeV)	σ_{fus} (mb)	System	$E_{c.m.}$ (MeV)	σ_{fus} (mb)
$^{16}O+^{70}Ge$	31.3	0.36(10)		41.8	452(17)
	32.1	1.63(23)		42.7	503(18)
	33.0	6.84(37)		43.5	581(17)
	33.8	19.98(97)		44.3	624(19)
	34.6	46.6(17)		45.1	660(13)
	35.4	86.7(33)		45.9	706(17)
	36.2	123.6(46)		46.7	770(33)
	37.1	187.0(72)		47.6	803(25)
	37.9	230.9(83)		47.6	798(24)
	38.7	287(10)		48.4	875(25)
	39.5	353(10)		49.2	933(27)
	40.3	405(14)		50.0	978(28)
	40.3	394(20)		50.8	1066(28)
	41.1	469(24)		51.6	1134(27)
	42.0	505(20)			
	42.8	565(21)	$^{16}O+^{73}Ge$	32.6	11.7(18)
	43.6	630(24)		33.4	25.7(26)
	44.4	680(26)		34.3	46.6(39)
	44.4	689(34)		35.1	79.1(54)
	45.2	704(29)		35.9	117.7(78)
	46.0	727(31)		36.7	157.3(96)
	46.9	797(29)		37.5	212(16)
	47.7	836(33)		38.4	249(14)
	48.5	863(34)		38.4	250(17)
	48.5	840(27)		39.2	328(15)
	48.5	848(29)		40.0	364(21)
				40.0	392(28)
$^{16}O+^{72}Ge$	31.3	0.41(8)		40.8	419(24)
	32.1	1.44(18)		40.8	436(25)
	32.9	4.69(27)		41.7	442(29)
	33.8	13.45(63)		42.5	547(19)
	34.6	31.7(15)		43.3	560(23)
	35.4	62.6(28)		44.1	630(26)
	36.1	90.3(33)		44.9	704(27)
	36.9	130.0(50)		45.8	706(24)
	37.7	180.1(66)		46.6	797(32)
	38.5	237(10)		47.4	859(37)
	39.3	274(10)		48.2	862(26)
	40.1	336(13)		49.0	882(28)
	40.1	330(14)		49.9	887(37)
	40.1	341(12)		50.7	992(34)
	40.9	394(10)		51.5	973(35)

measured points contribute to the determination of the depth parameter in the present procedure. For any given value of the fitting parameter, the nuclear ion-ion potential can be uniquely determined and, by combining it with the Coulomb potential for two-point charges, the fusion barrier can be also determined. In principle, we were thus able to perform calculations under any of three assumptions for the shape of each reactant: (a) it is spherical, in which case the treatment for a vibrational nucleus is applied, (b) it has a static oblate deformation ($\beta<0$), or (c) it has a static prolate deformation ($\beta>0$). In the latter two cases the equivalent-spheres approximation is used, without explicitly including any excited state of the reactant.

For the inelastic channels, all known states with a significant $E2$ or $E3$ transition strength to the ground state were taken into account. The relevant spectroscopic information is listed in Table IV, which contains exactly the same parameters used in Ref. [7] for the Ge isotopes and in Refs. [8,9] for ^{16}O. For calculations where a static deformation was used, the value of $|\beta_2|$ listed in Table IV for the corresponding lowest transition was used in each case, a procedure that can be justified within the adiabatic rotational model under the assumption of an axially symmetric nucleus. Since it is the deformation length $\beta_\lambda R$ that is the relevant quantity, all values of β_λ given in this paper were normalized to correspond to the standard radius given by (1).

TABLE III. Total fusion cross sections for $^{16}O+^{74,76}Ge$.

System	$E_{c.m.}$ (MeV)	σ_{fus} (mb)	System	$E_{c.m.}$ (MeV)	σ_{fus} (mb)
$^{16}O+^{74}Ge$	31.1	.47(1)	$^{16}O+^{76}Ge$	31.1	.60(15)
	31.9	1.67(27)		32.0	3.07(41)
	32.7	7.64(61)		32.8	9.90(74)
	33.5	19.8(13)		33.6	25.2(13)
	34.3	44.7(22)		34.5	57.6(26)
	35.2	76.7(39)		35.3	86.1(38)
	36.0	116.0(56)		36.1	132.3(54)
	36.8	164.5(82)		36.9	180.5(80)
	37.6	220.0(78)		37.8	236.0(90)
	38.5	256.3(73)		38.6	299(12)
	39.3	317.1(91)		39.4	388(15)
	40.1	346(11)		39.4	364(14)
	40.9	434(16)		40.3	404(15
	41.8	473(22)		41.1	426(17)
	42.6	553(26)		41.1	441(16)
	43.4	589(31)		41.9	473(19)
	44.2	631(26)		42.7	566(22)
	45.1	649(24)		43.6	606(25)
	45.9	722(28)		44.4	644(28)
	46.7	788(24)		45.2	691(26)
	47.5	754(24)		46.1	787(29)
	48.4	821(24)		46.9	820(31)
	49.2	868(26)		47.7	846(32)
	50.0	890(29)		48.5	907(35)
	50.8	932(29)		49.4	934(33)
	51.6	965(30)		50.2	988(38)
	52.5	989(28)		50.2	1000(32)
	53.3	964(27)		51.0	1090(30)
	54.1	1000(34)		51.8	1119(44)
				52.7	1138(44)
				53.5	1153(46)
				54.3	1207(46)

The ^{16}O nucleus, being doubly magic, is well known to have a spherical shape and therefore all calculations were performed under this assumption. For the Ge isotopes, on the other hand, calculations for all three model assumptions for the shape were made. The following shorthand notation is defined in order to label the different models: Two capital letters are used, the first referring to the projectile and the second to the target. Each letter can be either S, O, or P meaning that a spherical, an oblate deformed, or a prolate deformed shape is assumed for the nucleus, respectively. So, for example, a model calculation where a given Ge isotope is assumed to be oblate deformed is labeled SO, where the S serves only to emphasize the fact that the ^{16}O projectile is assumed to be spherical (vibrational).

IV. DISCUSSION

The values of χ^2 per degree of freedom obtained for each system under all three model assumptions are presented in Table V. The sensitivity of χ^2 to the model assumptions was not as good here as it was for the Al+Ge systems presented in Ref [7]. For the ^{16}O + $^{70,72}Ge$ systems, for example, the three curves (not shown) obtained for the excitation function with the SO, SP, and SS models are very close together and therefore the corresponding differences in Table V are not enough to discriminate against any of them. In any case, we see that for these two systems the SS model gives either the minimum value of χ^2, or close to it, so that the assumption of a spherical shape for $^{70,72}Ge$ is consistent both with the present results and with the conclusions of Ref. [7]. For the ^{16}O + ^{73}Ge system, on the other hand, the SS curve provides the best fit to the data, especially in the far sub-barrier region. This again is consistent with the conclusions of Ref. [7], where the superiority of the spherical model for ^{73}Ge over the oblate or prolate deformed models was even clearer. For the case of ^{16}O + ^{74}Ge the SS and SO curves practically coincide with each other and differ from the SP curve mainly in the region around the barrier, where the experimental error bars are barely enough to define a preference for the SP model. Finally, for the ^{16}O + ^{76}Ge system the SS and SO curves are practically identical and differ from the SP curve only for the three lowest energy points, where the SP curve is clearly better. These last conclusions of a prolate deformed shape for $^{74,76}Ge$ give again consistency with the conclusions drawn from the measurements for Al+Ge in Ref. [7].

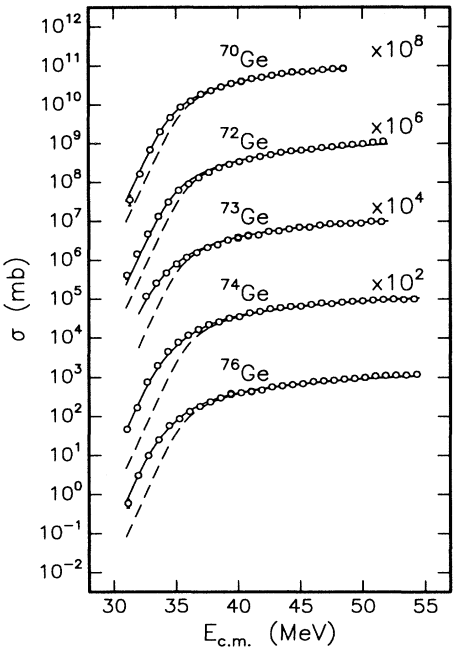

FIG. 3. Experimental fusion cross sections for ^{16}O + ^{70,72,73,74,76}Ge. The dashed curves correspond to one-dimensional barrier penetration calculations, while the solid curves are the results of the best-model calculations, as discussed in the text.

In order to investigate the role played by the assumed degrees of freedom for ^{16}O, we made calculations in which the degrees of freedom for the target or the projectile were artificially switched off for each system. The results are shown by the curves labeled p (dashes) and t (dots), respectively, in Figs. 4–8. The model sequences SS, SS, SS, SP, SP have been used in these figures to make the calculations for ^{16}O + ^{70,72,73,74,76}Ge, respectively. We can see that a common feature of all these calculations is that the p curves produce a similar enhancement for all targets, reflecting the fact that the same degrees of freedom are used for the projectile in each case. The t curves, on the other hand, do not follow the same pattern. For the ^{16}O + ^{70,72}Ge systems (Figs. 4 and 5), the t curves produce essentially the same enhancement as the p curves, except in the near barrier region where the p curves give the dominant enhancement. For both systems, it is clear from Figs. 4 and 5 that the target degrees of freedom by themselves (t curves) are not sufficient to properly describe the data and the addition of projectile degrees of freedom is necessary to obtain the observed enhancements.

For the ^{16}O + ^{73}Ge system, we see from Fig. 6 that the t curve produces a much larger enhancement than the p curve in the far sub-barrier region, a result which is a direct con-

TABLE IV. Inelastic channels included in the coupled-channels calculations and respective coupling parameters.

Nucleus	J^π	E_x (MeV)	λ	β_λ
^{16}O	2^+	6.92	2	0.37
	2^+	11.52	2	0.24
	3^-	6.13	3	0.70
^{70}Ge	2^+	1.04	2	0.23
	3^-	2.56	3	0.23
^{72}Ge	2^+	0.83	2	0.25
	3^-	2.51	3	0.24
^{73}Ge	$\frac{5}{2}^+$	0.013	2	0.24
	$\frac{7}{2}^+$	0.069	2	0.32
	$\frac{7}{2}^+$	0.499	2	0.13
	$\frac{13}{2}^+$	0.826	2	0.27
^{74}Ge	2^+	0.60	2	0.29
	3^-	2.54	3	0.16
^{76}Ge	2^+	0.56	2	0.27
	3^-	2.69	3	0.14

TABLE V. Value of χ^2 for the different model predictions for each system. O, P, and S in the first (second) place implies O(Ge) oblate, prolate, and spherical, respectively.

System	Model SO	SP	SS
^{16}O+^{70}Ge	1.8	2.3	1.5
^{16}O+^{72}Ge	5.4	3.4	3.7
^{16}O+^{73}Ge	2.9	2.3	1.8
^{16}O+^{74}Ge	4.6	3.5	5.4
^{16}O+^{76}Ge	3.8	3.1	3.8

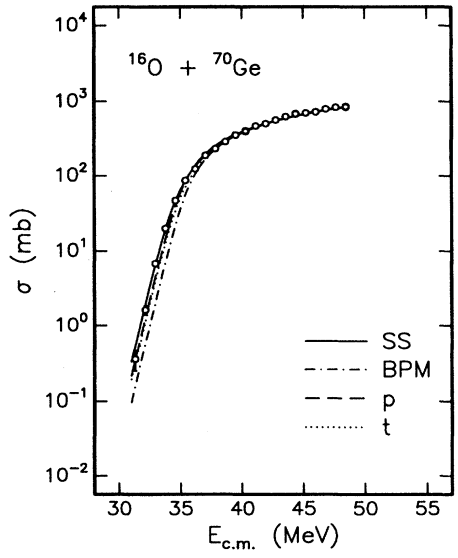

FIG. 4. Comparison of model calculations (curves) with experimental data (dots) for the ^{16}O + ^{70}Ge system. The solid curve is the result of the "best-model" calculation, as discussed in the text. Barrier penetration model (BPM) calculation. Only projectile (p) degrees of freedom considered. Only target (t) degrees of freedom considered.

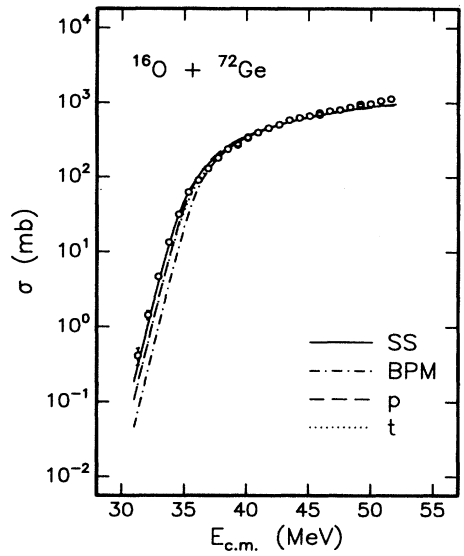

FIG. 5. Same as Fig. 4, but for the $^{16}O + ^{72}Ge$ system.

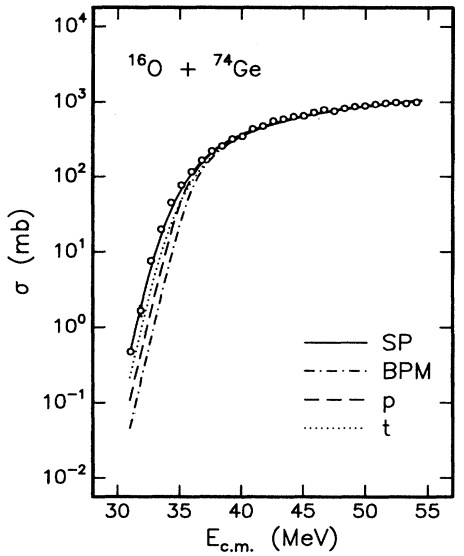

FIG. 7. Same as Fig. 4, but for the $^{16}O + ^{74}Ge$ system.

sequence of the larger number of favored channels and the low excitation energies of the states in the ^{73}Ge target, as can be seen from Table IV. The experimental enhancement is even larger than that produced by the t curve, however, and only when the degrees of freedom for ^{16}O are included in the calculation can the experimental points be properly described. A similar situation is observed for $^{16}O + ^{74,76}Ge$ in Figs. 7 and 8, but the enhancements produced by the t curves in the far sub-barrier region are here ascribed to the prolate deformation of both ^{74}Ge and ^{76}Ge. Again, the inclusion of the projectile degrees of freedom proves to be quite important in order to properly describe the data.

The possible effects of the coupling of two-phonon states in vibrational nuclei on fusion processes have been studied by several authors. Takigawa and Ikeda [24] used simplified coupled-channels calculations to show, in an analysis of the $^{58}Ni + ^{58}Ni$ and $^{74}Ge + ^{74}Ge$ systems, that this coupling introduces extra enhancement at low energies but reduces the enhancement at energies very close to the barrier. Esbensen and Landowne [25] then confirmed that a large part of the sub-barrier fusion cross sections observed in Ni + Ni systems can be accounted for by including higher-order vibrational couplings. More recently, Kruppa *et al.* [26] found, in a theoretical study of $^{16}O + ^{92}Zr$, that for this lighter system the inclusion of double identical phonons affects the excitation function only in the region where the cross sections are rapidly becoming unmeasurably small (below ~ 0.1 mb). The corresponding barrier distribution, however, seems to be significantly affected in an energy region where the cross sections can still be measured with some precision. Some

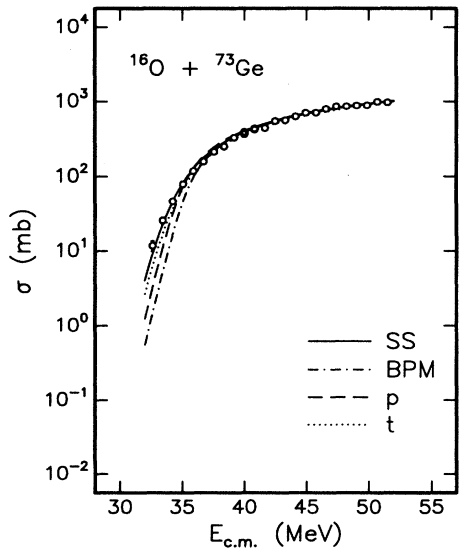

FIG. 6. Same as Fig. 4, but for the $^{16}O + ^{73}Ge$ system.

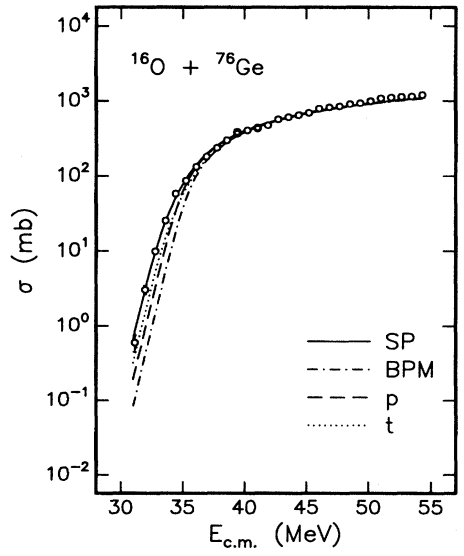

FIG. 8. Same as Fig. 4, but for the $^{16}O + ^{76}Ge$ system.

evidence has been found for two-phonon structure of the 0_2^+, 2_2^+, and 4_1^+ states in ^{70,72}Ge from proton [27,28], deuteron [29], and Li [28] scattering studies. One may thus ask about the possible effects of such states on the fusion of these nuclei with ^{16}O. Although CCDEF is able to take account of multiple phonon excitations, including two-phonon states formed by mutual excitation [26], those in which the same phonon is doubly excited cannot be handled with this code. A more complete coupled-channels calculation is beyond the scope of this work; we instead make the following qualitative argument: It is well known that the effects of coupling inelastic channels on the sub-barrier fusion cross sections are scaled according not only to the coupling parameters β but also to the height V_0 of the Coulomb barrier, since the change in barrier height associated with the coupling is proportional to the product βV_0 [30]. This could explain why the fusion excitation function for O + Zr from Ref. [26] is practically unaffected by the coupling of two identical-phonon states while that for the Ni + Ni system from Ref. [25] is considerably affected. Since our systems are even lighter than the one discussed in Ref. [26], while the corresponding deformation parameters are similar to those of ^{92}Zr, we might expect weaker or, at most, similar effects on our fusion calculations to those reported in that reference. In particular, the predicted fusion excitation functions for ^{16}O + ^{70,72,73}Ge in a coupled-channels calculation, where one- and two-phonon states are included for the target but no internal degree of freedom is assumed for the projectile, are expected to coincide with those shown by the t curves in Figs. 4–6, respectively. Therefore, as far as the excitation functions are concerned, two-phonon contributions would be irrelevant and our previous conclusions concerning the importance of the ^{16}O degrees of freedom for the three systems with vibrational targets hold. We will see later that the barrier distributions extracted from our data are also consistent with these conclusions.

In order to test for possible effects of higher-order deformations, a hexadecapole deformation was added for ^{74,76}Ge with β_4 values of 0.022 [31] and 0.02 [32], respectively. Disregarding ^{16}O degrees of freedom, a CCDEF fit was made to the data. For the ^{74}Ge target, the best fit gives something very similar to the t curve in Fig. 7, with $\chi^2 = 24.5$. So for this case the β_4 deformation is not able to explain the data as well as the inclusion of the ^{16}O degrees of freedom, which gave $\chi^2 = 3.5$ (Table V). For the ^{76}Ge target, on the other hand, a fairly good fit to the data was obtained, with $\chi^2 = 3.6$. This is almost as good as the value of 3.1 reported in Table V for the SP model. A possible way to discriminate against any of these models is provided by the barrier distribution, which we now explore for all measured systems.

It has been shown [33] that the distribution of fusion barriers can be deduced from the curvature $d^2(E\sigma)/dE^2$ of $E\sigma(E)$. A three-point formula with variable step was used to numerically evaluate second derivatives for our data. In order to keep statistical uncertainties at a reasonably low value, most of the derivatives were calculated using third nearest neighbors, except for the lowest and second lowest energy points for which it was necessary to use first and second nearest neighbors, respectively. The results are presented in Fig. 9 for all measured systems along with theoretical curves obtained by taking the numerical derivative of the CCDEF predictions for different models. Since the numerical derivatives may be quite sensitive to the step ΔE used to evaluate them, it is important to use the same ΔE for both the data and the theoretical predictions. We used $\Delta E = 0.8$ MeV (1.6 MeV) to obtain the derivatives in the region around the lowest (second lowest) energy data points, and $\Delta E = 2.5$ MeV for higher energies. The three curves thus obtained were then joined by straight lines. The sizes of the regions were chosen so as to obtain composite curves as smooth as possible, although this goal was not always achieved. In order to emphasize the importance of using appropriate values for ΔE, we show for comparison the curves obtained when a value $\Delta E = 0.1$ MeV was systematically used. For ^{70,72,73}Ge, the curves corresponding to the SS and t models of Figs. 4–6 are shown. For the two lighter systems, the SS model looks better around the peak and it predicts a long tail which also appears in the data. This tail is almost nonexistent in the predictions of the t model. For the ^{73}Ge target, on the other hand, the curves corresponding to both models are quite close to each other and therefore no apparent discrimination is provided by the barrier distribution for this case. Since the excitation function does actually distinguish between them, there is no ambiguity and we may conclude that, for the three vibrational targets, the analysis of barrier distributions gives results consistent with our previous conclusions; i.e., the SS model provides a good description of these data.

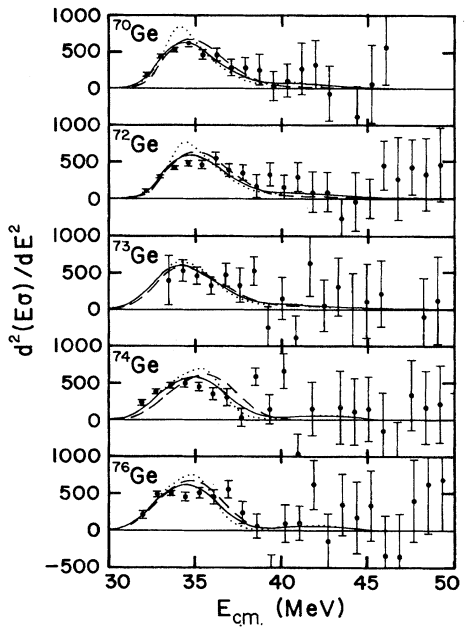

FIG. 9. Barrier distributions extracted from our data and CCDEF predictions for different models. Solid (dashed) lines correspond to the SS (t) model for ^{70,72,73}Ge and the SP ($t+\beta_4$) model for ^{74,76}Ge. The dotted and solid lines correspond to the same model but using different energy steps in the numerical derivatives.

Regarding the effects of two-phonon contributions on the barrier distributions, we must say that by using CCDEF we were not able to reproduce the shape predicted by the CCFUS calculations reported in Ref. [26] for the barrier distribution of ^{16}O + ^{92}Zr. Instead, the shape of the main peak corresponding to the more complete calculation in that reference,

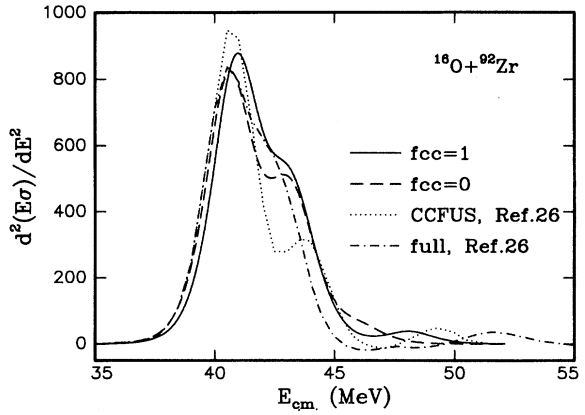

FIG. 10. CCDEF predictions for the barrier distribution of ^{16}O + ^{92}Zr, assuming no internal degree of freedom for ^{16}O. The states included in ^{92}Zr are 2^+ (E_x = 0.934 MeV, β_2 = 0.25) and 3^- (E_x = 2.339 MeV, β_3 = 0.17). The parameter fcc indicates the way the diagonalization is performed, as explained in the text. Also shown are the CCFUS results of Kruppa *et al.* and their calculations including double identical-phonon excitations.

including the two-phonon states $(2^+)^2$ and $(3^-)^2$ in ^{92}Zr, was fairly well reproduced. This would indicate that the inclusion of similar two-phonon states for $^{70,72,73}Ge$ should not change appreciably the shape of the t curves in Fig. 9 for these targets. However, the discrepancy with the CCFUS calculations of Ref. [26] is not understood since CCDEF is equivalent to CCFUS when no static deformation is considered and it was checked that the version we use does indeed reproduce the test run output reported for CCFUS in Ref. [34]. In our CCDEF calculations we did always use the option recommended for strong coupling (fcc=1), where a second order estimation of the position and height of the effective barriers is carried out within a 1 fm distance from the barrier position. When this condition was relaxed, allowing the code to diagonalize the coupling at the barrier position (fcc=0), the second bump observed in Ref. [26] began to appear but there still remains a qualitative difference between the two calculations, particularly in the relative heights of the two peaks in each calculation. The results of our CCDEF calculations for ^{16}O + ^{92}Zr are presented in Fig. 10 for comparison purposes, where the free parameter was fixed to reproduce the barrier height of 41.7 MeV from Ref. [26]. An energy step $\Delta E = 0.02$ MeV was used to evaluate the numerical derivatives. A larger step, such as that used for our data, would bring the curves to an even closer resemblance with the more complete calculation of Kruppa *et al.* [26] (dash-dotted line in Fig. 10).

Returning now to Fig. 9, the model that includes β_4 deformations in $^{74,76}Ge$ disregarding ^{16}O degrees of freedom, labeled $t + \beta_4$, predicts a peak shifted toward high energies with respect to the data for ^{74}Ge and the SP model is clearly better for this case. For the ^{76}Ge target the data seem to have a small structure that is not reproduced by either model, but this could be the effect of having only a marginal precision as far as the barrier distribution is concerned. The χ^2 values obtained from these calculations (3.0 for SP and 3.7 for $t+\beta_4$) favor the SP model. However, given the small difference between these values and also between those reported above for the corresponding excitation functions, perhaps the best argument to discriminate between these two models can be given by considering the global perspective of all analyzed systems. It would be extremely unusual for inelastic excitations of ^{16}O to play a significant role in fusion with $^{70,72,73,74}Ge$, but no role at all in the fusion with ^{76}Ge.

TABLE VI. Barrier parameters extracted from our data and from the systematics of Ref. [17].

	This work			Systematics	
System	R_0 (fm)	V_0 (MeV)	$\hbar\omega_0$ (MeV)	R_0 (fm)	V_0 (MeV)
$^{16}O+^{70}Ge$	9.8	35.0	3.9	9.7	35.1
$^{16}O+^{72}Ge$	9.7	35.4	3.9	9.8	34.9
$^{16}O+^{73}Ge$	9.9	34.9	3.9	9.8	34.8
$^{16}O+^{74}Ge$	9.7	35.4	3.9	9.8	34.7
$^{16}O+^{76}Ge$	9.8	35.0	3.8	9.9	34.5

The radius R_0, height V_0, and curvature parameter $\hbar\omega_0$ of the fusion barrier were calculated for each system under the assumptions that the $^{70,72,73}Ge$ isotopes are spherical while ^{74}Ge and ^{76}Ge are prolate deformed. These parameters, along with the corresponding results from the systematics reported in Ref. [35], are shown in Table VI. We see that the extracted barriers agree with those calculated from Ref. [35] to within better than 2%.

V. SUMMARY AND CONCLUSIONS

The near barrier and sub-barrier fusion cross sections for the ^{16}O + $^{70,72,73,74,76}Ge$ systems have been measured using a recoil velocity spectrometer. From systematic calculations in which inelastic vibrational channels were coupled to the ground state of spherical nuclei, while the equivalent-spheres method was used for deformed nuclei, a consistent scheme was found that properly described all features of the data, including the barrier distributions. The same degrees of freedom determined independently for O and Ge in previous works were used in these calculations. The shape transition between the spherical $^{70,72,73}Ge$ isotopes and the prolate deformed $^{74,76}Ge$ nuclei, deduced from the ^{27}Al + $^{70,72,73,74,76}Ge$ measurements in Ref. [7], was also observed in the present data, but with much-reduced sensitivity most likely resulting from the lower Z of the projectile used in the present work. This scheme is consistent [7] with previous systematic studies of neutron transfer reactions, Coulomb excitation, deuteron, proton, and α-particle scattering concerning the Ge isotopes. The larger enhancement associated with the ^{73}Ge target (with respect to that corresponding to $^{70,72}Ge$) reported in Ref. [7] was also evident in the O + Ge systems measured here. This supports the interpretation given there whereby the odd-A structure of ^{73}Ge provides more low-lying collective inelastic channels that can be coupled to the ground state with appreciable strength, which in turn produces a larger enhancement.

The role played by the projectile degrees of freedom was investigated by artificially decoupling the contributions of

target and projectile from the sub-barrier enhancement. The two contributions turned out to be equivalent for the two systems involving the ^{70,72}Ge isotopes, but the target contribution dominated for the three heavier systems and especially for the case of the ^{73}Ge target. However, the target contribution by itself was never sufficient to account for the experimental enhancement (except perhaps for ^{76}Ge; see below), and only when the two contributions were coupled together could the data be properly described. The inclusion of two-phonon states in vibrational targets was discussed in terms of a qualitative argument which shows that these degrees of freedom are most probably irrelevant for our systems. The model including a hexadecapole deformation of the target could not explain the data for the ^{16}O + ^{74}Ge system but it gave a fairly good description for ^{16}O + ^{76}Ge. Although the data favored the model including the ^{16}O degrees of freedom for this system by only a small margin, this is also the most reasonable model within the framework of the global analysis of all measured systems. It is interesting to note that, even though ^{16}O excitations have not directly been observed in inelastic scattering experiments with Ge targets [36], they do seem to provide important doorway states to fusion for these systems. Previous analysis of O + Sm fusion data [8,9,12] did actually show very important contributions of the ^{16}O internal degrees of freedom to the sub-barrier enhancements. In a study of inelastic scattering of ^{16}O + ^{152}Sm [37], the possible effects of channels corresponding to ^{16}O excitations in the coupled-channels calculations were disregarded. It might well be that, in addition to being weak channels because of the high energies of the first states in ^{16}O, the absorption from them into fusion is so strong at sub-barrier energies that the scattering channels are practically depleted. More complete coupled-channels calculations [17] performed for elastic and inelastic scattering of ^{16}O on ^{40,48}Ca, ^{58}Ni, and ^{88}Sr do indeed support this hypothesis.

ACKNOWLEDGMENTS

One of the authors (E.F.A.) wishes to thank the University of Notre Dame for allowing several stays in the Nuclear Structure Laboratory. This work was partially supported by CONACYT (Mexico) and by the U.S. National Science Foundation.

[1] *Heavy Ion Collisions at Energies Near the Coulomb Barrier*, Proceedings of the Workshop, Daresbury, U.K., 1990, edited by M. A. Nagarajan, IOP Conf. Proc. No. 110 (Institute of Physics and Physical Society, London, 1990).
[2] S. Landowne, S. C. Pieper, and F. Videbaek, Phys. Rev. C **35**, 597 (1987).
[3] R. A. Broglia, C. Dasso, and S. Landowne, Phys. Rev. C **32**, 1426 (1985); G. Pollarolo, in Ref. [1], p. 37.
[4] R. G. Stokstad and E. E. Gross, Phys. Rev. C **23**, 281 (1981).
[5] P. H. Stelson, in Ref. [1], p. 191.
[6] P. O. Hess and P. Pereyra, Phys. Rev. C **42**, 1632 (1990).
[7] E. F. Aguilera, J. J. Vega, J. J. Kolata, A. Morsad, R. G. Tighe, and X. J. Kong, Phys. Rev. C **41**, 910 (1990).
[8] E. F. Aguilera, J. J. Vega, J. J. Kolata, A. Morsad, and R. J. Tighe, Notas Fis. **13**, 1 (1990); in Proceedings of the Thirteen Oaxtepec Symposium on Nuclear Physics, Mexico (unpublished).
[9] E. F. Aguilera, Rev. Mex. Fis. **38**, Supl. 2, 1 (1992).
[10] R. G. Stokstad, Y Eisen, S. Kaplanis, D. Pelte, V. Smilansky, and I. Tserruya, Phys. Rev. C **21**, 2427 (1980).
[11] D. E. DiGregorio, M. diTada, D. Abriola, M. Elgue, A. Etchegoyen, J. O. Fernandez Niello, A. M. J. Ferrero, S. Gil, A. O. Macchiavelli, A. J. Pacheco, J. E. Testoni, P. R. Silveira Gomes, V. R. Vanin, R. Jiguori Neto, E. Crema, and R. G. Stokstad, Phys. Rev. C **39**, 516 (1989).
[12] P. R. S. Gomes, I. C. Charret, R. Wanis, G. M. Sigaud, V. R. Vanin, R. Liguori Neto, D. Abriola, O. A. Capurro, D. E. DiGregorio, M. di Tada, G. Duchene, M. Elgue, A. Etchegoyen, J. O. Fernandez Niello, A. M. J. Ferrero, S. Gil, A. O. Machiavelli, A. J. Pacheco, and J. E. Testoni, Phys. Rev. C **49**, 245 (1994).
[13] J. X. Wei, J. R. Leigh, D. J. Hinde, J. O. Newton, R. C. Lemmon, S. Elfstrom, J. X. Chen, and N. Rowley, Phys. Rev. Lett. **67**, 3368 (1991).
[14] J. R. Leigh, N. Rowley, R. C. Lemmon, D. J. Hinde, J. O. Newton, J. X. Wei, J. C. Mein, C. R. Morton, S. Kuyucak, and A. T. Kruppa, Phys. Rev. C **47**, R47 (1993).
[15] T. Izumoto, T. Udagawa, and B. T. Kim, Phys. Rev. C **51**, 761 (1995).
[16] C. R. Morton, M. Dasgupta, D. J. Hinde, J. R. Leigh, R. C. Lemmon, J. P. Lestone, J. C. Mein, J. O. Newton, H. Timmers, N. Rowley, and A. T. Kruppa, Phys. Rev. Lett. **72**, 4074 (1994).
[17] H. Esbensen and F. Videbaek, Phys. Rev. C **40**, 126 (1989).
[18] E. F. Aguilera, J. J. Vega, J. J. Kolata, and R. J. Tighe, Rev. Mex. Fis. **38**, Supl. 1, 63 (1992).
[19] J. J. Vega, E. F. Aguilera, G. Murillo, J. J. Kolata, A. Morsad, and X. J. Kong, Phys. Rev. C **42**, 947 (1990).
[20] E. F. Aguilera, J. J. Vega, E. Martinez, J. J. Kolata, and A. Morsad, Rev. Mex. Fis. **35**, 489 (1989).
[21] P. Sigmund and K. B. Winterbon, Nucl. Instrum. Methods **119**, 541 (1974).
[22] J. Fernandez Niello, C. H. Dasso, and S. Landowne, Comput. Phys. Commun. **54**, 409 (1989).
[23] C. Y. Wong, Phys. Rev. Lett. **31**, 766 (1973).
[24] N. Takigawa and T. Ikeda, in Proceedings of the Symposium on the Many Facets of Heavy Ion Reactions, edited by W. Henning *et al.*, Report. No. ANL-PHYS-86-1 (unpublished), p. 613.
[25] H. Esbensen and S. Landowne, Phys. Rev. C **35**, 2090 (1987); Nucl. Phys. **A492**, 473 (1989).
[26] A. T. Kruppa, P. Romain, M. A. Nagarajan, and N. Rowley, Nucl. Phys. **A560**, 845 (1993).
[27] T. H. Curtis, H. F. Lutz, and W. Bartolini, Phys. Rev. C **1**, 1418 (1970).
[28] J. Jabbour, L. H. Rosier, E. I. Obiajunwa, and B. Ramstein, Nucl. Phys. **A500**, 356 (1989).

[29] G. Szaloky, L. A. Montestruque, M. C. Cobian-Rozak, and S. E. Darden, Phys. Rev. C **18**, 750 (1978).
[30] R. Lindsay and N. Rowley, J. Phys. G **10**, 805 (1984).
[31] L. H. Rosier and E. I. Obiajunwa, Nucl. Phys. **A500**, 323 (1989).
[32] B. Ramstein, R. Tamisier, L. H. Rosier, and P. Avignon, Nucl. Phys. **A411**, 231 (1983).
[33] N. Rowley, G. R. Satchler, and P. Stelson, Phys. Lett. B **254**, 25 (1991).
[34] C. H. Dasso and S. Landowne, Comput. Phys. Commun. **54**, 409 (1989).
[35] L. C. Vaz, J. M. Alexander, and G. R. Satchler, Phys. Rep. **69**, 373 (1981).
[36] M. E. Cobern, N. Lisbona, and M. C. Mermaz, Phys. Rev. C **13**, 674 (1976); C. D. Uhlhorn, B. Gonsior, D. Wegner, K. P. Lieb, H. H. Wolter, and A. M. Kleinfeld, Z. Phys. A **311**, 79 (1983).
[37] B. T. Kim, Phys. Lett. **80**, 353 (1979).